Crustal fissuring on the crest of the southern East Pacific Rise at 17°15′–40′S

Dawn J. Wright
Department of Geosciences, Oregon State University, Corvallis, Oregon, USA

Rachel M. Haymon, Scott M. White,[1] and Ken C. Macdonald
Department of Geological Sciences, University of California, Santa Barbara, California, USA

Received 30 March 2001; revised 8 December 2001; accepted 13 December 2001; published 31 May 2002.

[1] Fissure densities and widths have been mapped along the axial zone of the superfast spreading southern East Pacific Rise (EPR) at 17°15′–40′S with the near-bottom DSL-120 and *Argo II* imaging systems. We observe that the youngest lava flows (on a relative age scale) are sparsely fissured and that there is a cumulative increase in fissure abundance with time that produces a strong positive correlation between fissure density and relative age of lava flows. Average fissure widths were used to estimate fissure depths. In the 17°15′–40′S area, calculated fissure depths are estimated to extend below the seismic layer 2A/2B boundary, and fissures are widest/deepest where lava flows are youngest. We interpret these wide fissures in relatively young flows to be eruptive fissures. Relatively young lava flows combined with high average fissure widths south of 17°25′S suggest that there may have been recent dike propagation along the ridge crest in this area. In comparison to the northern EPR at 9°–10°N the density of fissuring on the southern EPR is significantly higher, due in part to the higher occurrence of relatively older, more areally restricted pillow lava flows. *INDEX TERMS:* 3035 Marine Geology and Geophysics: Midocean ridge processes; 3045 Marine Geology and Geophysics: Seafloor morphology and bottom photography; 8010 Structural Geology: Fractures and faults; *KEYWORDS:* fissures, fractures, mid-ocean ridges, southern East Pacific Rise, tectonic cycle

1. Introduction

[2] The superfast spreading southern East Pacific Rise (EPR) exhibits a number of features that make it different from slower spreading mid-ocean ridges (MORs), including its relatively long segments, separated by infrequent and small offsets; an inflated cross section; pronounced asymmetry in spreading rate and subsidence; and an abundance of off-axis lava flows and seamounts [*Scheirer et al.*, 1996a, 1998]. Still poorly understood are the along-axis extent and frequency of diking events and eruptions, as well as the width of the subsurface dike intrusion zone (although the recent Autonomous Benthic Explorer data of *Cormier et al.* [1999] and *Shah et al.* [1999] are shedding light on this). On other parts of the MOR and in Iceland much attention has been given to the study of dikes (i.e., magma-filled cracks), mainly in connection to faulting and magmatism [e.g., *Gudmundsson*, 1990; *Karson et al.*, 1992; *Rubin*, 1992; *Johnson and Salem*, 1994; *Lowell and Germanovich*, 1995; *Dziak et al.*, 1995]. However, in order to fully understand the nature of mechanical failure in an extensional environment, one must also consider the location, distribution, and geometry of fissures, which provide essential pathways into the upper oceanic crust through which magma and hydrothermal fluids may migrate. In the past this has been difficult on the MOR because of the lack of good quality data at the scale of meters to tens of meters. *Crane* [1987] was the first to tabulate fissure abundance and length along the axial zone of the EPR (using the side-looking sonars of the deep-towed Sea MARC I with selectable swath widths of 1.5, 3, and 6 km at 10°35′ to 13°10′N). No further studies focusing primarily on fissures were performed on any part of the MOR until the 1989 *Argo I* survey of the northern East Pacific Rise (EPR) at 9°12′–54′N [*Wright et al.*, 1995a, 1995b] and the 1994 *Argo II* survey of the Trans-Atlantic Geotraverse (TAG) active hydrothermal mound at 26°N on the Mid-Atlantic Ridge [*Bohnenstiehl and Kleinrock*, 2000]. These surveys provided the first, and at present the only, data sets that were of sufficient density, continuity, and geographical precision to meaningfully map and analyze fissure distributions at a fine scale, along with distributions of hydrothermal vents, lava flows, and biological communities [e.g., *Haymon et al.*, 1991].

[3] In this study we present an analysis of fissure characteristics along the superfast spreading southern EPR and compare the results to those obtained previously along the fast spreading northern EPR. We used the high-resolution, near-bottom imaging capabilities of the *Argo II* optical/acoustical system and the DSL-120 deep-towed sonar system to establish the abundance, widths, and spatial distribution of fissures, as well as the estimated depth of fissuring, along the axial zone of the southern EPR at 17°15′–40′S (the ''Spike survey'') and 18°23′–30′S (the ''Hump survey''). Statistical analyses characterize fissure density, width, length, and depth on both a third- and fourth-order segment scale. These finer scales of segmentation are typically characterized at the third-order scale by very small overlapping spreading centers (OSCs; offset less than ~1 km), local topographic lows (saddle points), or small deviations from axial linearity (Devals); and at the fourth-order scale by even smaller Devals (offset <200 m), intravolcano gaps and offsets of axial summit troughs or calderas (*White et al.* [2000] as modified from *Macdonald et al.* [1991]). Analysis of the spatial dimensions of fissures at these segment scales is critical to understanding the processes controlling their geometry. Fissures may either be of magmatic origin (forming above subsurface dikes that

[1]Now at Department of Geological Sciences, University of South Carolina, Columbia, South Carolina, USA.

0148-0227/02/2001JB000544$09.00

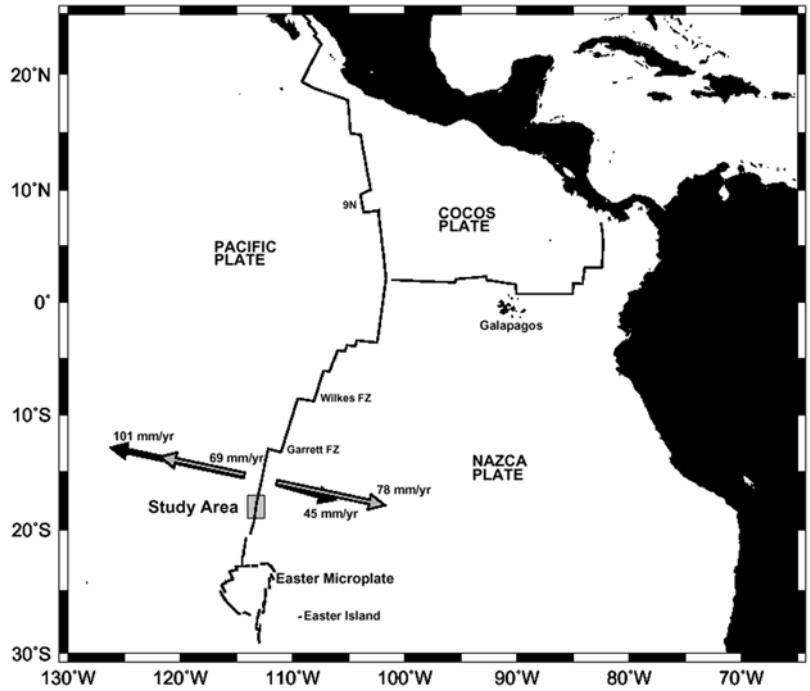

Figure 1. Regional location map of the study area (marked by shaded box) on the southern EPR. Plate boundaries are from *Cormier et al.* [1996]. Arrows near study area are Pacific-Nazca plate motion vectors [after *Cormier et al.*, 1996]. Solid arrows represent absolute motion, and shaded arrows indicate relative motion. Overall, the Pacific Plate is moving significantly faster over the hot spot reference frame than the Nazca Plate (101 versus 45 mm/yr) [*Gripp and Gordon* [1990]. Because both the absolute and relative plate motion directions are nearly ridge perpendicular, the EPR axis is migrating by ~30 mm/yr to the WNW over the hot spot frame of reference [*Scheirer et al.*, 1996a]. At the ridge axis, spreading is significantly faster to the east than to the west [e.g., *Naar and Hey*, 1989; *Perram et al.*, 1993; *Hey et al.*, 1995]. Since 1 Ma, the average Pacific rate of spreading has been ~69 mm/yr, while the average Nazca rate has been ~78 mm/yr; full spreading rate is ~147 mm/yr [*Cormier et al.*, 1996].

sometimes reach the seafloor and erupt) or tectonic origin (forming in response to lateral tensional stress), reflective of tumescence/detumescence (inflation/deflation of ridge axis over a magma chamber), or thermal contraction (shrinkage of cooling rock). With the passage of time, fissure abundance may increase [*Wright et al.*, 1995a, 1995b], and existing fissures may widen by mass wasting of their margins, or by extension.

2. Geological Setting

[4] The southern EPR (Figure 1) has been the focus of numerous surveys and geophysical experiments, particularly between the Garrett Fracture Zone and the propagating ridge at 20.7°S [e.g., *Lonsdale*, 1989; *Macdonald et al.*, 1988; *Scheirer et al.*, 1996a, 1996b; *Magde et al.*, 1995; *Carbotte et al.*, 1997; *Scheirer et al.*, 1998]. This section of ridge is ~800 km long, representing a remarkably uninterrupted, long-wavelength undulation in axial depth. Major morphotectonic/magmatic segments separated by six OSCs and one Deval, have been previously identified. All are in varying stages of tectonic, magmatic, and hydrothermal development [e.g., *Lonsdale*, 1989; *Sinton et al.*, 1991; *Auzende et al.*, 1996; *Cormier et al.*, 1996; *Scheirer et al.*, 1996a]. The ridge axis is offset on a finer scale by a series of small, en echelon, left-stepping discontinuities ranging in offset from 1 to 7 km [*Cormier et al.*, 1996]. The ridge segments in between these offsets all strike consistently within a few degrees of 013°, which is normal to the direction of spreading predicted by the NUVEL-1A model of current plate motions [*DeMets et al.*, 1994].

[5] North of an OSC at 19°S, the ridge axis is particularly robust magmatically, as evidenced by its shallow, broad, inflated cross section [e.g., *Scheirer and Macdonald*, 1993; *Cormier and Macdonald*, 1994] and abundant hydrothermal activity [e.g., *Bäcker et al.*, 1985; *Renard et al.*, 1985; *Marchig et al.*, 1986; *Auzende et al.*, 1996; *Baker and Urabe*, 1996]. Seismic data show a strong reflection from the top of the axial magma chamber (AMC), which is generally ~1 km below the seafloor, as opposed to the 1.2–1.6 km depth typical of the northern EPR [*Detrick et al.*, 1993; *Mutter et al.*, 1995]. However, the morphology of the ridge crest changes drastically between the two second-order segments north and south of the OSC at 17°56′S [*Ballard and Francheteau*, 1982; *Renard et al.*, 1985; *Lonsdale*, 1989; *Auzende et al.*, 1996]. Between 16°30′S and 17°56′S the ridge has a broad, domed cross section that is widest and most shallow at ~17°25′S [*Renard et al.*, 1985; *Auzende et al.*, 1996]. The seismic data of *Detrick et al.* [1993] at this location show that the AMC changes dramatically along-strike from a flat-topped body at relatively constant depth to a peaked cupola (''spike'') that intrudes to within 800 m of the seafloor, thus representing the most extreme along-strike thermal gradient to be documented along any portion of the global MOR. For example, if it is assumed that the temperature of melt at the top of the magma chamber is ~1200°C [*Lin and Parmentier*, 1989], then the vertical temperature gradient in this region changes from ~900 to ~1200°C/km over a distance of <5 km, and from ~900 to ~1700°C/km over ~30 km. *Mutter et al.* [1995] have interpreted this as seismic evidence for an axial eruption in progress. Indeed, subsequent to these seismic surveys, a 1993 *Nautile* dive series from 16°30′S to 17°56′S found extremely young lava flows containing numerous collapse pits, as well as a general absence of fissures in these relatively young flows [*Auzende et al.*, 1996]. Similar observations were made in 1994 and 1997 with the *Shinkai 6500* [*Fujioka et al.*, 1995; *Urabe et al.*, 1995; *Embley*, 1998] and

in 1998 with *Alvin* [*Sinton et al.*, 1999]. A 1996 survey of the ridge crest with the DSL-120 deep-towed sonar (see below) revealed the presence of two narrow (<50 m wide) collapse troughs at 17°26′–29′S (Aldo Lake Trough) and 17°42′–45′S (Pisco Trough) [*Haymon et al.*, 1997; R. M. Haymon et al., manuscript in preparation, 2001]. *Macdonald and Fox* [1988], *Haymon* [1996], and *Lagabrielle and Cormier* [1999] have suggested that some, if not most, axial summit troughs (ASTs) along both the northern and southern EPR represent elongate collapse calderas formed above magma chambers, rather than rifted features resulting from stages of dominantly amagmatic extension. The AST at 17°26′–29′S represents drainback during the waning phases of an eruption in the AST model of *Fornari et al.* [1998] (stage 1b of 4).

[6] In contrast to the northern section of ridge at 16°30′–17°56′S, the 75-km section to the south is notched by a prominent trough bisecting the axial high, varying in width from 500 to 2000 m and reaching up to 100 m in depth [*Ballard and Francheteau*, 1982; *Lonsdale*, 1989; *Lagabrielle and Cormier*, 1999]. The ridge from 17°56′ to a 3-km-wide OSC at 18°22′S is primarily a half graben. The next 25 km from 18°22′S to 18°35′S is known as the ''Hump'' because of its markedly convex topographic profile along-axis. Observations made here by various *Nautile* dive series [*Bäcker et al.*, 1985; *Renard et al.*, 1985; *Auzende et al.*, 1996], and later confirmed by the *Argo II* survey of *Haymon et al.* [1997], indicate that the trough is floored throughout with lava flows that are cut by numerous fissures and buried by talus near the walls.

3. Data Acquisition and Analysis

[7] In late 1996, the *Argo II* and DSL-120 seafloor imaging systems [*Bowen et al.*, 1993; *Scheirer et al.*, 2000] were used to conduct a near-bottom survey of the narrow (<500-m-wide) axial zone of the southern EPR from 17°15′S to 18°30′S (135 km; Figure 1). This study focuses on the *Argo II* survey at 17°15′–40′S [*Haymon et al.*, 1997]. Initially, the DSL-120 was used above the seafloor to collect 120-kHz sidelooking acoustic reflectance and phase bathymetry data within a continuous, 1-km zone of ridge crest (towing height of ~75 m yielding an imagery swath of ~1000 m) [*White et al.*, 2000]. *Argo II* was then towed at ~6–10 m above the seafloor to conduct dense visual, acoustic (200 kHz), magnetic, and water column surveys within the DSL-120 sonar survey area, first at Spike and finally at Hump. Fifteen axis-parallel lines through the axial zone with line spacings of 10–30 m (see R. M. Haymon et al. (manuscript in preparation, 2001) for track line maps) provided 80–100% visual coverage where the axial zone is <100 m wide, down to a minimum coverage of ~45% where the axial zone widens at 17°25′S. The maximum width imaged within the Spike survey area was ~700 m.

[8] Calculations were made of the area of axial zone visually imaged during the *Argo II* survey, based on the field of view of its forward looking camera (~16 m at 9 m above the seafloor), which provides a greater swath width than the downlooking cameras. The calculations are based on the geographic information system buffering and clipping procedures established by *Wright et al.* [1995a] but further take into account the varying altitude of *Argo II*. R. M. Haymon et al. (manuscript in preparation, 2001) more fully discusses the characteristics of all cameras and instruments used on *Argo II*. These calculations were necessary for an accurate determination of fissure density, which, after *Wright et al.* [1995a, 1995b], is defined as the number of fissures per square kilometer of seafloor visually imaged. For the current study, fissures were counted and measured from *Argo II* forward looking video, electronic still camera (ESC) photography (Figure 2), and cross-track Imagenex, 675-kHz, mechanical sonar traces. Processing of the video and ESC data, analysis, and histogram construction follow the methodology of *Wright et al.* [1995a]. Features within, but much larger than, the field of view of the *Argo II* cameras were digitized in their entirety from DSL-120 side-scan records

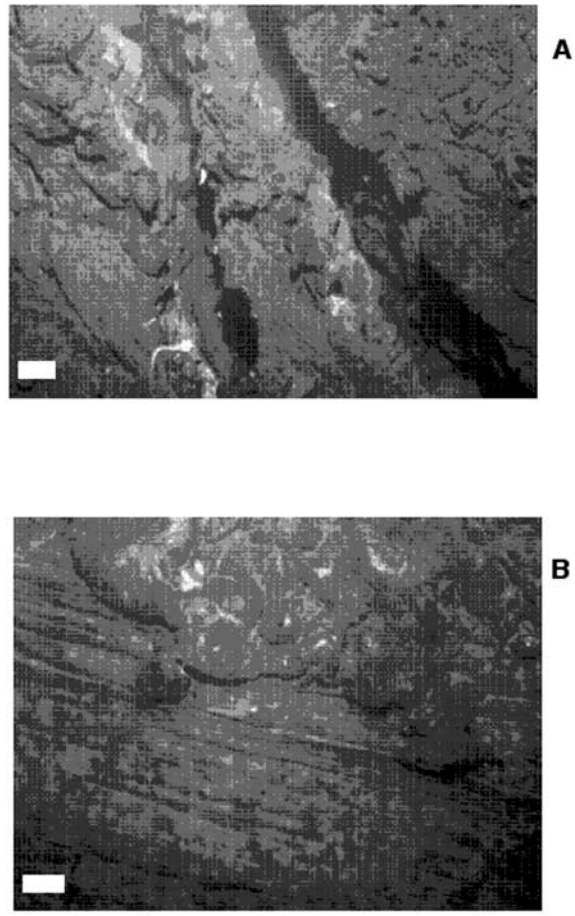

Figure 2. (a) *Argo II* electronic still camera image of two 1-m-wide fissures in relatively young (age 1) autobrecciated sheet flow along the axial zone of the Aldo Lake Segment, 17°28′S. Depth ~2600 m, altitude ~6.5 m. Scale bar at lower left is 1 m. (b) *Argo II* electronic still camera image of a contact between young (age 1) sheet flow underlying an age 1 lobate flow in the axial zone of the Tubeworm Segment, 17°30.5′S. Depth ~2600 m, altitude ~6.0 m. Scale bar at lower left is 1 m.

(see *White et al.* [2000] for representative images), and the digitized coordinates inspected to ensure that counts of these features were not duplicated in counts from the visual observables and Imagenex records. Histograms and graphs illustrating the density, width, and depth of fissures include data from all three observables: video, ESC, Imagenex, and side-scan sonar.

[9] The 1996 *Argo II* survey at Hump covered only a limited portion of that second-order segment (i.e., 9 of the 25 km), which limits its usefulness for correlating fissure properties with fine-scale morphotectonic segmentation. There is also evidence that the Hump region has a more complex history than the Spike region, including periods of amagmatic extension, and possible massive collapse [*Lagabrielle and Cormier*, 1999]. The accumulation of fissure populations from these diverse processes makes the fissure patterns complicated. As a visual survey of the entire second-order segment is needed before detailed interpretations should be attempted, only data and interpretations for the Spike area are presented here.

4. Observations and Calculations

4.1. Distribution, Abundance and Widths of Fissures

[10] A total of 1630 fissures (1383 detected by *Argo II* video, ESC, and Imagenex plus 247 additional fissures detected by DSL-

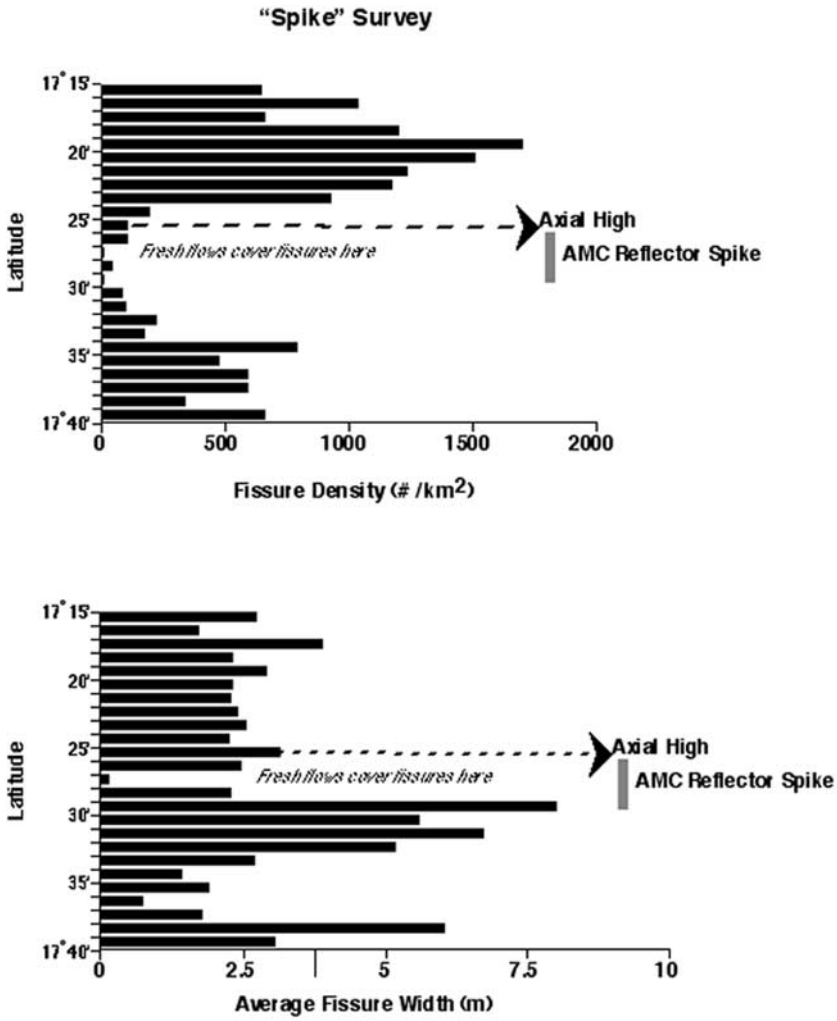

Figure 3. Variation along the ridge axis in fissure density and width for the southern EPR crest at 17°15′–40′S. (top) Density of fissures per square kilometer of seafloor visually imaged. (bottom) Average width of fissures (m) in bins of 1′ latitude. Vertical, solid bars to the right of the histograms indicate latitudinal extent of AMC reflector spike [*Mutter et al.*, 1995]. Dashed lines point to the locations of topographic highs along the axis (measured from walls).

120 sonar) were observed in the Spike survey area. Taking into account the heights of the *Argo II* vehicle off the bottom, the mean width of fissures detected by video, ESC, and Imagenex is 1.4 m (minimum width of 0.1 m, maximum width of 15 m). A systematic increase in fissure widths away from the ridge axis was not observed. Because of the spatial limitations inherent in video and ESC, lengths were not determined for the population of fissures observed in the video and ESC (nor by the Imagenex traces). The mean width of the larger fissures detected by DSL-120 sonar is 8 m, and the mean length is 111 m. All but four of the observed fissures were oriented parallel to the ridge axis.

[11] Figure 3 shows a pattern of more abundant, narrower fissures per unit area north of the axial high and the AMC reflector spike, trending to fewer and wider fissures south of it. The fewest number of fissures are found at 17°27′–28′S. This region is centered on the AMC reflector spike where the freshest, youngest-looking lava flows are found (age 0.5 on a scale of 0 = youngest → 2 = oldest [*Haymon et al.*, 1991, also manuscript in preparation, 2001]).These young, uncracked flows are probably covering preexisting fissures [*Haymon et al.*, 1997; *Sinton et al.*, 1999; R. M. Haymon et al., manuscript in preparation, 2001] (Figure 4). A region of very wide fissures is found at 17°27′–32′S, above and just south of the AMC reflector spike.

[12] Density and widths of fissuring correlate well with relative age distribution of axial lava flows throughout most of the Spike survey area (Figures 4 and 5). North of 17°23′S, there is a significant increase in both inferred relative lava ages and fissure densities, along with a significant decrease in mean fissure widths (Figures 3 and 4). Similar to previous findings on the northern EPR [*Wright et al.*, 1995a], the most densely fissured region lies in the oldest, age 2 terrain at 17°18′–21′S within a third-order discontinuity boundary zone [*White et al.*, 2000], while the least fissured areas at 17°25′–29′S are presumably very young (ages 0 to 0.5; Figures 3–5). A small region of age 2 axial lavas south of 17°38′S, although populated with numerous fissures, is not as densely fissured as the age 2 lavas north of the AMC reflector spike (Figure 4).

[13] Figure 5 shows a strong correlation between fissure density and relative lava age within the Spike survey area and also shows a measured fissure density that is several times higher than that found along the northern EPR at 9–10°N. Although video, ESC, and Imagenex observations from *Argo II* are included in the data points for Spike (Figure 5), while only video observations from *Argo I* are included for the 9–10°N data (Figure 5), the fissures observed by ESC and Imagenex in the Spike area augment the total number of fissures by <15% and

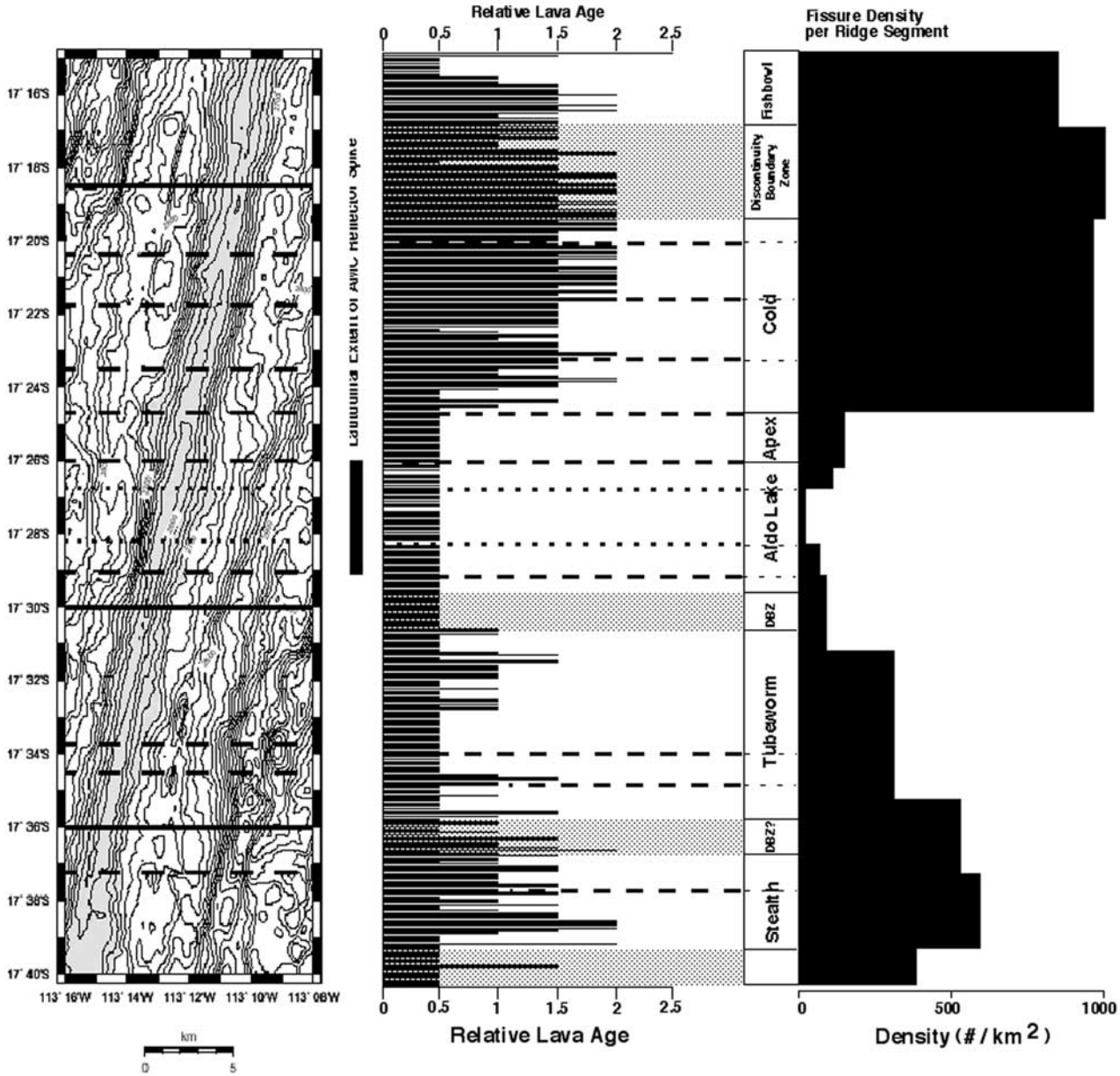

Figure 4. Distribution of tectonic and volcanic features along the southern EPR crest at 17°15′–40′S, modified from R. M. Haymon et al. (manuscript in preparation, 2001). Bathymetric contour interval is 20 m, from the Sea Beam 2000 data of *Scheirer et al.* [1996b]. Shading indicates areas shallower than 2700 m. Solid horizontal lines over bathymetry indicate central latitudes of distinct third-order discontinuities [after *White et al.*, 2000], dashed lines indicate distinct fourth-order discontinuities, and dotted lines indicate potential fourth-order discontinuities (both after *White et al.* [2001]). Vertical, solid bar to the right of bathymetry indicates latitudinal extent of AMC reflector spike [*Mutter et al.*, 1995]. Moving to the right, the next column shows the along-axis variation in inferred relative lava age (after R. M. Haymon et al., manuscript in preparation, 2001). Each small histogram bar represents the minimum relative lava age within a 100-m latitudinal bin. Third-order discontinuities are shaded zones (including discontinuity boundary zones, DBZs), distinct fourth-order discontinuities are dashed lines, and potential fourth-order discontinuities are dotted lines. The last two columns show the locations of ''Deval''-bounded ridge segments, as determined by *White et al.* [2001], and a horizontal histogram of the fissure density per ridge segment.

cannot explain the observed fivefold increase in the density of fissures when compared to the density of fissures along the northern EPR. We speculate that the observed difference in fissure density between the northern and southern EPR survey areas is due to a comparatively greater proportion of young sheet flows that have poured out of the more extensive axial summit collapse troughs present along the EPR at 9°–10°N (see discussion section below).

4.2. Estimates of Fissure Depth

[14] The depth of a fissure (also referred to here as ''crack depth'') is a valuable piece of information because it has implica-

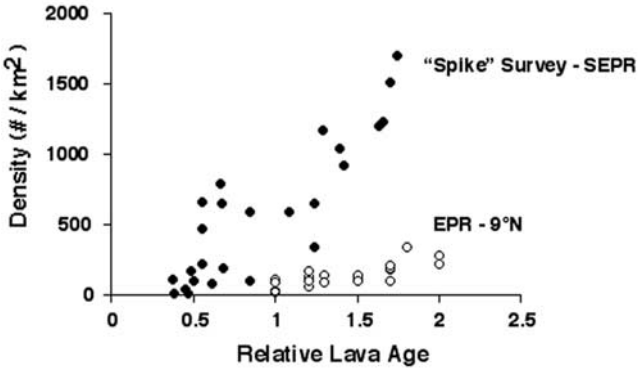

Figure 5. Fissure density versus relative lava age for 17°15′–40′S (solid symbols), compared to 9°12′–54′N (open symbols). EPR 9°N data from *Wright et al.* [1995a]. Relative lava ages were averaged within the same latitudinal bins as fissure density. Note how much higher fissure density is along the southern EPR.

tions for the mechanical conditions under which the fissure formed and hence about the history of the rock in which it occurred [*Lachenbruch*, 1961]. The deeper the penetration of fissures, the more important their role in crustal tectonics. For example, deep fissures serve as conduits for magma emplacement and increase the permeability of the upper crust for the mobility of hydrothermal fluids. This in turn has a profound effect on the mechanical behavior of the crust and on its effective strength at depth.

[15] *Wright* [1998, and references therein], *Fialko* [2001], and *Garel et al.* [2002] review the mechanics of fissure formation in volcanic rift zones and describe in detail the background theory, relevant mechanical factors (i.e., elastic moduli, tensile stress, and tensile strength of the host rock) and simple fracture mechanics models applicable to fissure formation and development at fast spreading mid-ocean ridges. An initial caveat is that these models are primarily two dimensional and assume that oceanic crust is uniform, isotropic, and elastic. Seismic velocity, electrical resistivity or deep borehole investigations (such as the recent borehole televiewer studies of *Krammer et al.* [1995] and *Ito* [1995]) may eventually be adequate to determine the actual depth distribution of cracks within the study area. However, until in situ determinations or a rigorous three-dimensional analytical solution for anisotropic, heterogeneous ocean crust become available, one must rely on a two-dimensional solution, using reasonable values for the linear elasticity and density of the rock. These two-dimensional models do, however, rest on a substantial body of experimental information obtained with terrestrial rocks, metals, plastics, glass, and concrete and have met with success in subaerial studies and engineering applications [*Wright et al.*, 1995b].

[16] *Wright et al.* [1995b] employed a width-to-depth relation for fissures observed along the axial zone of the EPR at 9–10°N with *Argo I.* Because the dimensions of fissures in the Spike survey area are very similar to those mapped at 9–10°N in terms of width, length, and mechanics of formation, estimates of crack depth follow the same assumptions and crack depth model used by *Wright et al.* [1995b]. The assumptions are that (1) oceanic basement is a uniform, isotropic, elastic medium; (2) fissures are of finite dimensions, where the width of the fissure may be controlled either by its depth or its length; and (3) cracking is of a ''top down'' mode where a fissure initiates at the surface (i.e., is not initially filled with magma) and the depth of penetration is related to the width of opening. The crack depth model is a variation on the plane stress model of *Tada et al.* [1973] and *Gudmundsson and Bäckström* [1991], as implemented by *Wright et al.* [1995b]:

$$z_0 = \frac{E_w}{\sigma V_1(d/b)}, \tag{1}$$

where is z_0 estimated crack depth, E is Young's modulus, w is fissure width, and σ is the tensile stress at the time of crack formation. $V_1(d/b)$ is the stress function of *Tada et al.* [1973]:

$$V_1(d/b) = \frac{1.46 + 3.42[1 - \cos(\pi/2)(d/b)]}{[\cos(\pi/2)(d/b)]^2}. \tag{2}$$

In the stress function above, d is 300 m (in accordance with a calculated estimate of z_{max}, after the methodology of *Wright et al.* [1995b]), and b is the brittle thickness of the crust, which translates to ~1200 m for the southern EPR [*Hussenoeder et al.*, 1996]. Adopted or calculated values for these parameters are shown in Table 1. *Wright et al.* [1995b] explain the theoretical background on these parameters and present explanatory formulas related to estimates of fissure depth. Again, the models, and the depth estimates resulting from it, are limited by the assumption of crustal uniformity, as we know that there are indeed substantial changes in the physical properties of the crust with depth all the way down to the AMC. However, many of these changes are still undetermined for the study area. An example is the calculation of the Young's modulus (E) parameter for equation (1), which should be 0.5 of a dynamic modulus, as determined from seismic results. The relation, given by *Jaeger and Cook* [1979], is

$$E_d = V_p^2 \rho \frac{(1+\nu)(1-2\nu)}{(1-\nu)}, \tag{3}$$

where E_d is the dynamic Young's modulus, V_p is P wave velocity, ν is a static Poisson's ratio, and ρ is rock density (Table 1). *Shaw* [1994] points out that the dynamic Poisson's ratio remains largely unknown due to the difficulty in obtaining direct shear wave velocity measurements in young ocean crust, especially in the uppermost portion. In order to approximate the in situ value, one must therefore rely on a static Poisson's ratio determined from laboratory measurements of basalt. For the southern EPR, *Collier and Singh* [1998] determined a Poisson's ratio of 0.48, but this applies only to the upper 50 m of crust within layer 2A; and the value decays to 0.35 approaching a subbottom depth of 200 m. On the EPR at 9°–10° N, *Christeson et al.* [1994, 1997] used on-bottom seismic refraction data to determine a minimum Poisson's ratio of 0.43 at the seafloor. Similarly, a P wave velocity of 4650 m s^{-1} may be adopted as an average for the uppermost 1 km of crust along the southern EPR [*Hussenoeder et al.*, 1996] (Table 1), but the P wave velocity in the upper 50 m that is appropriate for surface fissuring, and for surface Poisson's ratios of 0.48 or 0.43, is only 2–2.5 km s^{-1}. Therefore, because our chosen model is directly proportional to Young's modulus, there remains great uncertainty in the actual depth and extent of fissuring.

[17] The uncertainty is illustrated in Figure 6, which shows three estimates of along-strike crack depth variation for the Spike survey area. Crack depths were derived from the average crack width (i.e., the average widths of fissures within bins of 1 arc min latitude along-strike; Figure 3) and were based on reasonable combinations of Poisson's ratios with P wave velocities (Table 1) in the calculation of a Young's modulus for equation (1). Figure 6 shows the maximum, median, and minimum crack depths resulting from the model calculations, therefore giving a clearer picture of actual uncertainly. Also shown are the depths to the seafloor, the base of seismic layer 2A, and the AMC reflector (Figure 6). The layer 2A and AMC profiles are reproduced from the depth profiles of *Hooft et al.* [1997] and *Mutter et al.* [1995], respectively.

[18] The model used predicts crack depths ranging from ~10 to 400 m below seafloor, and near 17°30s, where crack widths are the greatest (as shown in Figure 3), all of the crack depth estimates penetrate the layer 2A/2B boundary. This does not correspond exactly with the location of the AMC reflector spike or the high-temperature vents (Figure 7), but it is several kilometers to the

Table 1. Elastic Moduli and Related Parameters Used for Estimates of Fissure Depth[a]

Parameter	Definition	Value	Units	Reference(s)
b	thickness of crust (for Tada's stress function only)	1200 ± 100	m	*Lin and Parmentier* [1989] and *Hussenoeder et al.* [1996]
E	static Young's modulus	980 ± 1000 (ν = 0.48, V_p = 2.5) 3400 ± 1000 (ν = 0.48, V_p = 4.65) 5400 ± 1000 (ν = 0.35, V_p = 2.5) 18,500 ± 1000 (ν = 0.35, V_p = 4.65)	Mpa	this study
g	acceleration of gravity	9.8	m s^{-2}	
T_0	rock tensile strength	3+3/−2	MPa	*Haimson and Rummel* [1982] and *Gudmundsson* [1992]
V_1 (d/b)	Tada's stress function	2.56	dimensionless	this study
V_p (near surface)	average P wave velocity of uppermost 50 m	2500 ± 400	m s^{-1}	*Hussenoeder et al.* [1996]
V_p (at depth)	average P wave velocity of uppermost 1 km	4650 ± 400	m s^{-1}	*Hussenoeder et al.* [1996]
w	crack width	0.1−30.0	m	this study
z_{max}, d	maximum depth of absolute tension	300 ± 100	mbsf (m below seafloor)	this study
z_0	crack depth	to be estimated	mbsf	this study
ν	Poisson's ratio	0.48 0.35 0.43 (EPR 9° N)	MPa	*Collier and Singh* [1998], *Christeson et al.* [1994], and *Wright et al.* [1995b]
ρ	average rock density of uppermost 1 km	2750 ± 100	kg m^{-3}	*Hussenoeder et al.* [1996]
σ	tensile stress at time of crack formation	30 ±10	MPa	*Lachenbruch* [1973]

[a] See *Wright* [1998, and references therein] and *Wright et al.* [1995b] for background equations involving these parameters and a full explanation of how they affect estimates of fissure depth at fast spreading mid-ocean ridges.

south of it. It is interesting to note that some cracks may have resulted from ponding and drainback of lava, which would have widened the surface widths of the fissures and resulted in overestimates of crack depth. Most of the collapse features in the survey area were identified in *Argo II* video records between 17°23′S and 17°27′S. However, most of the wide cracks in the 17°30′S region (averaging 8 m in width) were identified on DSL 120 sonar records, and it was very difficult to distinguish between

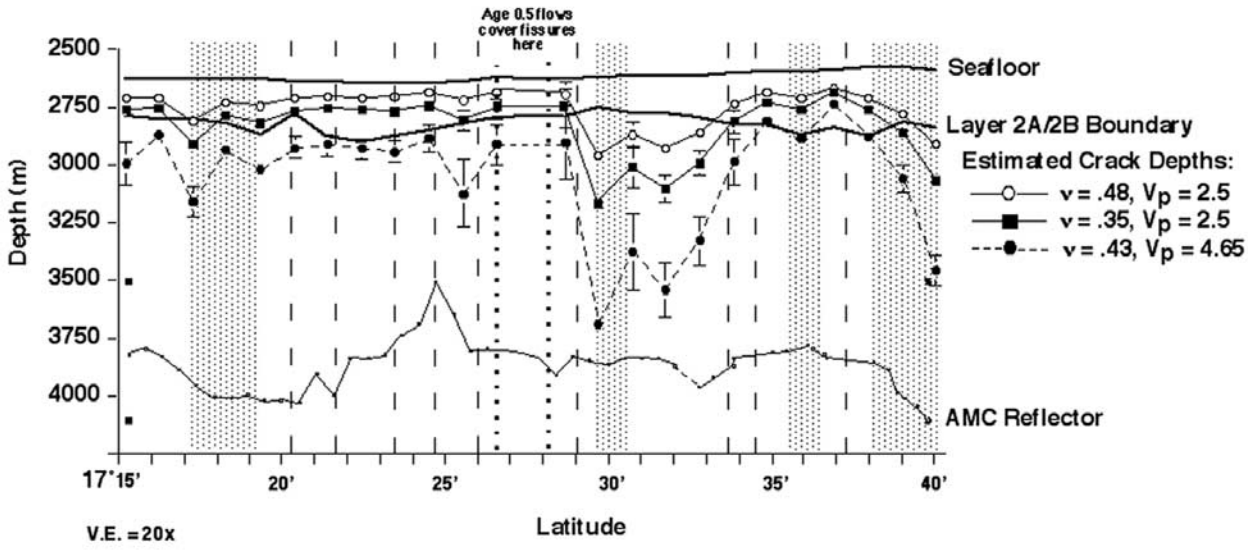

Figure 6. Estimates of along-strike crack depth at 17°15′–40′S based on the average widths of fissures, and using Poisson's ratios of 0.35, 0.48 [*Collier and Singh*, 1998], and 0.43 [*Christeson et al.*, 1994; *Wright et al.*, 1995b] and P wave velocities of 2.5 and 4.56 km/s [*Hussenoeder et al.*, 1996]. Errors bars on the depth estimates represent the standard errors of crack widths (i.e., standard deviations of the mean). The seafloor profiles are from the Sea Beam 2000 bathymetry of *Scheirer et al.* [1996b]; the ''layer 2A/2B boundary'' profiles are from *Hooft et al.* [1997]; and the ''AMC reflector'' profiles are from *Mutter et al.* [1995] and *Hooft et al.* [1997]. Vertical exaggeration is 20X. Shaded vertical bars mark the latitudes of third-order discontinuities [*White et al.*, 2000], including discontinuity boundary zones [*White et al.*, 2001]. Dashed vertical lines mark the latitudes of distinct fourth-order discontinuities; dotted lines the latitudes of potential fourth-order discontinuities [*White et al.*, 2001].

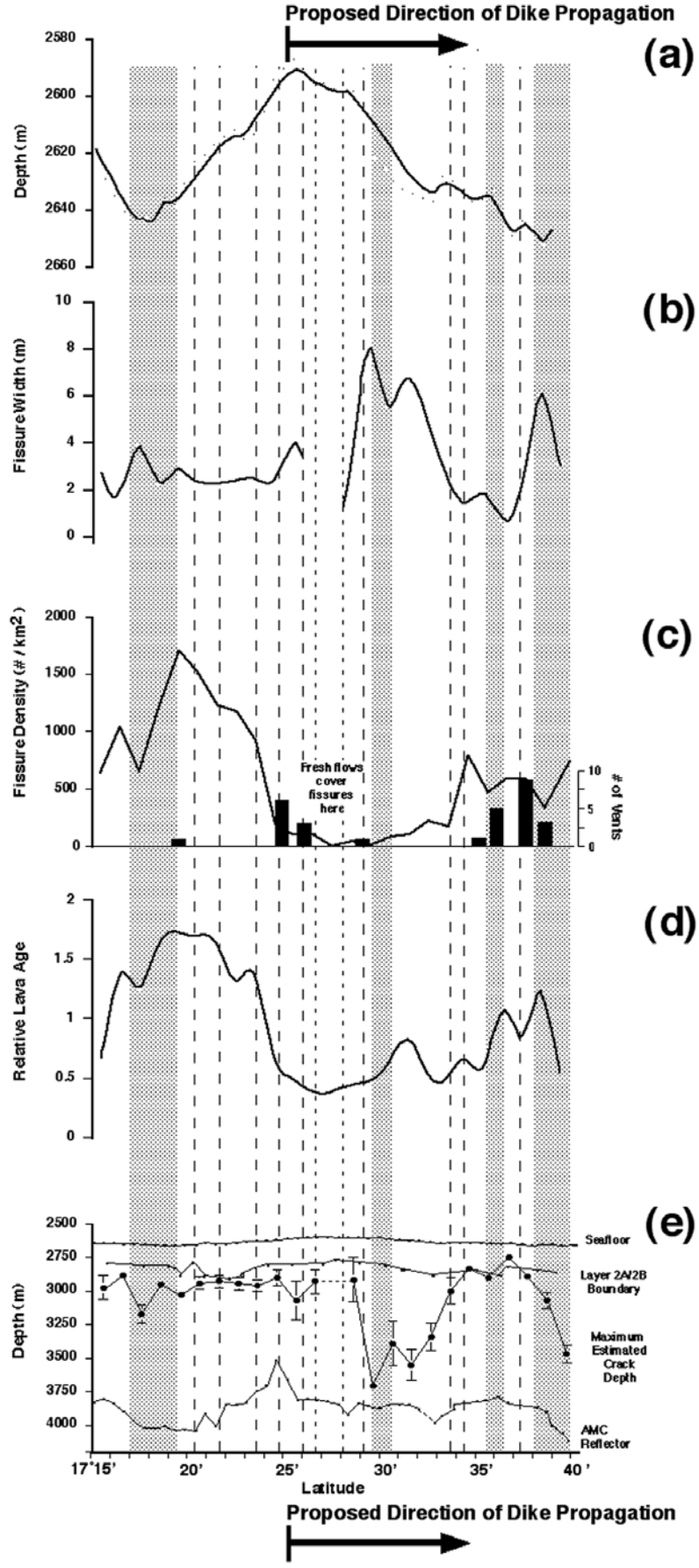
Proposed Direction of Dike Propagation
(a)
Depth (m)
2580
2600
2620
2640
2660
(b)
Fissure Width (m)
10
8
6
4
2
0
(c)
Fissure Density (# / km2)
2000
1500
1000
500
0
Fresh flows cover fissures here
10
5
0
# of Vents
(d)
Relative Lava Age
2
1.5
1
0.5
0
(e)
Depth (m)
2500
2750
3000
3250
3500
3750
4000
Seafloor
Layer 2A/2B Boundary
Maximum Estimated Crack Depth
AMC Reflector
17°15'
20'
25'
30'
35'
40'
Latitude
Proposed Direction of Dike Propagation

cracks that may have been widened due to collapse versus those that were not. The only region where cracks are not predicted to penetrate the layer 2A/2B boundary is just south of the third-order discontinuity at 17°37′S. Abundant hydrothermal activity is found immediately to the north and south of this region (Figure 7). For cracks predicted by the model to penetrate the layer 2A/2B boundary the estimated depths are considerably greater than those predicted for the EPR at 9–10°N [*Wright et al.*, 1995b], as well as those directly observed in the eroded Tertiary and Pleistocene lava piles of the rift zone in southwest Iceland [*Gudmundsson*, 1987; *Forslund and Gudmundsson*, 1991].

5. Discussion

5.1. Some Volcanotectonic Similarities Between the Fast and Superfast Spreading EPR

[19] Several studies [e.g., *Macdonald et al.*, 1988; *Rubin*, 1992; *Batiza*, 1996; *Baker and Urabe*, 1996; *Haymon*, 1996; *Head et al.*, 1996; *Chadwick and Embley*, 1998; *Curewitz and Karson*, 1998; *Fornari et al.*, 1998] provide convincing evidence for the dominant role of dike intrusion and lateral magma transport (over that of a simple far-field plate stress model) in generating cracks within the neovolcanic zone at both fast and superfast spreading ridges. Moreover, *Haymon* [1996] notes the excellent degree of correlation between magma budget and hydrothermal flux on both segment and global scales, bolstering the notion that magma supply exerts primary control on hydrothermal flux magnitude and vent distribution. However, at superfast spreading ridges the question remains whether the dike propagation is primarily lateral (from along-strike magma transport) or vertical (from the greater abundance/frequency of eruptions in spatially distributed areas). The magnitude and distribution of fissuring at superfast spreading ridges are largely governed by the episodic inflation and deflation of the ridge axis due to variations in dike propagation that may be lateral from a single injection point over an inflated magma reservoir, where most of the preexisting fissures are buried by recent eruptions.

[20] For example, along the northern EPR at 9–10°N, *Wright et al.* [1995a] found that the mean density of fissuring on a given fourth-order segment was greater where relative axial lava age was greater and that fissure density also correlated well with hydrothermal vent abundance and type. It was also found that the widest cracks (lower in density) occurred in the youngest lavas, suggesting that these cracks were eruptive in origin and controlled the locations of high-temperature hydrothermal venting. It was suggested that in these regions, average fissure widths and depths (found by *Wright et al.* [1995b] to be directly proportional to the widths) increase due to ridge crest inflation and lateral dike propagation, resulting from recent magmatic replenishment of the AMC from upper mantle sources. As was found on the fast spreading EPR at 9°–10°N, the most densely fissured regions in both the Spike and Hump surveys lie within relatively older (age 2) terrains, while the least fissured areas coincide with where the freshest lavas are found (Figure 7). This is particularly the case southward from the axial depth minimum and AMC reflector spike at 17°25′–29′S, where relative lava ages, average fissure widths and fissure depths all increase together along-strike. These observations may be consistent with a southward propagation of dikes along-strike away from a focused site of melt injection at 17° 25′–29′S. A second zone of southward dike propagation may start within the Stealth segment, between 17°37′S and 17°39′S, where young, age 1 axial lavas are again found (Figures 4 and 7d) as well as wide cracks and an abundance of hydrothermal activity (Figures 7b and 7c). It is surmised that magma migrating south from these injection sites erupted, pooled, and drained back to create the wider fissures that are observed, and the very large fissure depths that we estimate. More than 60% of the focused hydrothermal vents observed in the area are found along these wide, deep cracks [*O'Neill*, 1998; *O'Neill et al.*, 1998], which is similar to what was observed at 9–10°N where cracks are also widest/deepest in regions of eruption and venting.

[21] The numerical modeling of *Head et al.* [1996] shows that typical dike widths for the MOR should range from ~0.2 to ~3 m. Field observations at Hess Deep [*Francheteau et al.*, 1992; *Karson et al.*, 1992, 1999] and in the Oman ophiolite [*MacLeod and Rothery*, 1992] suggest that dikes along fast spreading ridges are indeed within this range, at 1 m. The experiments of *Mastin and Pollard* [1988] demonstrate that the top of a dike must be shallower than ~10 times its thickness at its top in order to generate fissures. *Head et al.* [1996] find that dikes in the range of 0.2–3 m thickness will cause fissuring at the surface only if they penetrate to depths of less than a few tens of meters. Dikes greater in thickness may be able to produce fissuring from much greater depths, given that the ambient stress at depth is near the level required for tensile failure. To wit, the dike propagation model of *Pollard et al.* [1983] for the 1976 Krafla fissure eruptions in Iceland places a dike of thickness ≥2 m at a depth of 250 m. The ambient stress at this depth must be near the level required for tensile failure of the crust (~30 MPa) in order for fissures to form above the dike at the surface [*Wright*, 1998]. Our estimates of fissure depth for the Spike survey area (mean depth of ~300 ± 60 m; Figure 6) therefore imply the presence of a number of failed dikes that were emplaced much deeper than predicted by the *Mastin and Pollard* [1988] model and may be of thicknesses in excess of 2–3 m. Preliminary confirmation of this has been found at Aldo Lake with Autonomous Benthic Explorer (ABE) magnetic and bathymetric data of *Cormier et al.* [1999]. In addition, *Cormier et al.* [1999] noted that the lips of a 20- to 50-m-wide, 200- to 500-m-long eruptive fissure in Aldo Lake were at a constant depth throughout, indicating that the magma rose to the same head everywhere from a well-connected magma source along axis. If southern EPR fissures are unconstrained by either the upper surface of the dike [*Rubin and Pollard*, 1987; *Rubin*, 1992] or the compressive stress field that forms normal to the dike (as was found for TAG fissures by *Bohnenstiehl and Kleinrock* [2000]), they may be forming in front of laterally propagating dikes. It should be noted that the Krafla event in Iceland, although involving dike emplacement at similar depths, was unusually voluminous, resulting in a zone of fissuring and faulting ~6 km wide

Figure 7. (opposite) Stacked plots (versus latitude) of axial topography, average fissure width, fissure density (overlain with focused hydrothermal flow), relative axial lava age, and estimated fissure depth for the southern EPR crest, 17°15′–40′S. Shaded vertical bars mark the latitudes of third-order discontinuities [*White et al.*, 2000], including discontinuity boundary zones [*White et al.*, 2001]. Dashed vertical lines mark the latitudes of distinct fourth-order discontinuities, dotted lines the latitudes of potential fourth-order discontinuities (R. M. Haymon et al., manuscript in preparation, 2001). (a) Smoothed axial depth profile of the ridge axis, from the Sea Beam 2000 data of *Scheirer et al.* [1996b]. Vertical exaggeration is 50X. (b) Interpolated profile of average and fissure width measured within bins of 1 arc min of latitude along-strike. (c) Along-strike variation in fissure density. *Argo II* observations of focused hydrothermal flow (i.e., high-temperature smokers and smoke plumes) are overlain for comparison [*Haymon et al.*, 1997; *O'Neill et al.*, 1998]. (d) Along-strike variation in relative axial lava age averaged within bins of 1 arc min of latitude along strike (data from R. M. Haymon et al. (manuscript in preparation, 2001)). (e) Maximum, estimated along-strike variation in crack depth from Figure 6. The ''seafloor'' and ''layer 2A/2B boundary'' profiles are also the same as in Figure 6. Error bars represent the standard errors. Vertical exaggeration is 20X.

[*Sigurdsson*, 1980], much larger than a typical neovolcanic zone on the MOR. However, *Curewitz and Karson* [1998] surmise that the intrusion of even a single 1-m dike on a fast spreading ridge should affect an area larger than the width of the axial region, though narrower than typical rift valleys at slow spreading ridges.

[22] As was observed at 9–10°N, positive correlation of fissure density with relative ages of axial lavas in the Spike area (Figure 4) reveals the tendency of the crust in the axial zone to accumulate more cracks with time rather than to widen existing cracks [*Wright et al.*, 1995a]. This implies that the formation of wide, deep cracks is intimately related to episodes of dike intrusion, the possibility of dike propagation that is lateral, the eruption of fresh, uncracked flows, and hydrothermal venting. Because of the greater frequency of eruptions at superfast spreading ridges, many of which are probably short-lived [*Sinton et al.*, 1999], lateral propagation may not necessarily extend as far along-strike (i.e., for tens of kilometers), as has been postulated for intermediate centers [e.g., *Chadwick and Embley*, 1998]. As intrusions and eruptions wane, magma drainback leads to the production of subcrustal voids, which help to collapse the crustal carapace and bring the onset of crustal cooling and extension (e.g., as described by *Engels* [2001]). This, in turn, produces additional smaller, shallower cracks in the frozen volcanic carapace overlying the sheeted dikes.

5.2. Some Volcanotectonic Differences Between the Fast and Superfast Spreading EPR

[23] Assuming that the mechanics of fracturing are the same at both the northern and southern EPR and that both are inflated sections of ridge (e.g., as evidenced by similarly large cross-sectional areas [*Scheirer and Macdonald*, 1992]), it is interesting to note several volcanotectonic differences between the two as evidenced by our data. In other words, processes do not necessarily remain the same as the spreading rate is scaled up.

[24] For instance, along the EPR at 9–10°N, *Wright et al.* [1995a] found a reasonably clear demarcation between ridge segments dominated by tectonic cracks versus eruptive fissures. While eruptive fissures cannot be unequivocally distinguished from those of purely tectonic origin using the *Argo II* images, fissures south of 17°25′S within the Spike survey area may indeed be eruptive in origin, due to the strong correlation of wide fissures in relatively young lava flows (Figures 4 and 7). Purely tectonic fissures, accumulated on axis in relatively older lava flows, would become wider as they move off axis, due to accumulated extension over time. Most of the fissures in the Spike survey area appear to penetrate the layer 2A/2B boundary (Figures 6 and 7) and are thus deep enough to tap melt and serve as loci for high-temperature hydrothermal discharge above dike intrusions (subject to tensile stresses opening pathways for hydrothermal flow ahead of and above a laterally propagating dike tip, as mentioned earlier). It is not evident that the narrowest fissures observed in this region have all formed in response to crustal extension and/or thermal contraction because a good proportion of them, in addition to extending well into layer 2B, occur in relatively young flows, age 0.5 to age 1 (Figures 4 and 7). This is not to imply, however, that it is impossible for a fissure at a superfast spreading ridge to be tectonic in origin if it penetrates the layer 2A/2B boundary. *Gudmundsson and Bäckström* [1991] have shown that a tectonic crack may extend as far as 500–800 m into the crust before developing into a normal fault. In contrast, observational evidence gathered at 9–10°N shows an abundance of narrower, shallower fissures in relatively older lava flows to be primarily tectonic, forming primarily within layer 2A [*Wright et al.*, 1995a, 1995b]. Also, within the Spike area, there is no clear demarcation between older lavas to the north or south of an axial high. For example, Figure 4 shows many pockets of relatively old age 2 lavas sandwiched in between lavas of age 1 and 1.5 throughout the Spike survey region. Eruptions at superfast spreading rates may be occurring in multiple segments all at once (along with the intrusion of many noneruptive dikes), so that a clear demarcation between older segments with abundant tectonic cracks and younger segments dominated by eruptive fissuring would be difficult to detect.

[25] An interesting observation is that while the most densely fissured regions in both the Spike and Hump survey areas lie within relatively older (age 2) terrains, the Spike region throughout has fissure densities far surpassing those of the northern EPR (Figure 5). This suggests that the relative lava ages within the surveyed zone of the southern EPR crest are older on average than the lava ages within the surveyed zone along the northern EPR. Because we are observing relative, rather than absolute, lava ages in both areas, we cannot test this hypothesis directly. However, we note in this context that lava flow morphology observations in the two areas reveals a much higher percentage of lobate and sheet flows relative to pillow flows along the northern EPR in comparison to the southern EPR [*White et al.*, 2000, 2002]. This is consistent with the much greater extent along strike of axial summit collapse troughs along the EPR at 9°–10°N, from which many lobate and sheet flows are emanating [*Kurras et al.*, 2000; *White et al.*, 2002; D. Fornari et al., AHA-NEMO2, Shipboard data web site compiled during R/V *Melville* NEMO expedition, Leg 2, WHOI, http://ahanemo2.whoi.edu, 2000]. We therefore postulate that a larger portion of the surveyed area on the northern EPR is covered by relatively young and uncracked lobate and sheet flows which are areally extensive, in comparison to the surveyed area on the southern EPR crest, which includes more areally restricted pillow lava flows that are on average older and hence more fissured. In fact, a key difference between fast and superfast spreading ridges may be the greater abundance/frequency of dikes at superfast ridges on a time-integrated basis, which may also help to explain the relative abundance of pillow lavas on the southern EPR. Because of the greater frequency of eruptions at superfast spreading rates, there may be a greater percentage of dikes that do not make it to the surface, and the dikes do reach the surface may have less magmatic head, resulting in eruptions that are less effusive, particularly at the ends of third-order segments.

[26] Another possible factor is that within the Spike survey area layer 2A is quite thin at the ridge axis [*Carbotte et al.*, 1997; *White et al.*, 2000]. *White et al.* [2000] have noted that this is the case because the axial high here is an isostatic rise instead of a constructional volcanic ridge. A thinner crust at superfast spreading rates may cause cracking events to accelerate and propagate much farther, which would increase crack density and also could activate multiple fine-scale segments at once. For example, the average layer 2A thickness along the axis in the Spike survey area is ~25% thinner than it is on the EPR axis at 9°–10°N (~140 m; Figure 6), compared to ~175 m at EPR 9.5°N [*Christeson et al.*, 1994]. Fissures at superfast spreading rates may form and move so quickly from the leading edge of a laterally propagating dike that they are not constrained by segment boundaries, as they are at fast spreading rates.

[27] *Haymon et al.* [1991] and *Wright et al.* [1995a] have shown how the structure of a fast spreading ridge crest is related to both magmatic and tectonic processes that may be episodically cyclic within a second-, third- or fourth-order segment. The model of *Haymon et al.* [1991] for 9–10°N describes individual fourth-order segments in different phases of a volcanic-hydrothermal-tectonic cycle on a 100- to 1000-year timescale, beginning with episode(s) of cracking/diking and eruptive fissuring, followed by magmatic drainback, gravitational collapse, possible development of an AST, and then cooling of the heat source, initiation of tectonic fissuring, and waning of hydrothermal and magmatic activity.

[28] It is not evident that along-strike variability in crustal fissuring corresponds as closely to the fine-scale morphotectonic segmentation of the ridge crest as on the northern EPR at 9–10°N, where fine-scale segment boundaries coincide almost exactly with along-strike changes in the mean density of fissuring, in relative ages of axial lavas, and also in hydrothermal vent abundance

[*Haymon et al.*, 1991; *Wright et al.*, 1995a, 1995b]. *White et al.* [2000] found systematic changes in volcanic morphology at the third-order scale and proposed that each third-order segment physically behaves as a single volcanic system, with higher effusion rates near segment centers and lower effusion rates near segment ends. Why the volcanic expression does not translate to clear signatures in crustal fissuring remains unclear. *Rubin et al.* [2001] have found that the chemical heterogeneity of lavas at 17°26′–27′S is indicative of a fissure eruption with an initially slow effusion rate, followed by a much higher effusion rate near the end. They surmise that the last phase of the eruption may have covered most of the lavas initially erupted, making it difficult to distinguish between along-axis compositional patterns and zonations within the flow [*Rubin et al.*, 2001]. So perhaps what distinct signatures there may be in the variability of fissuring at fine-scale segment boundaries are constantly being covered by new flows.

6. Summary and Conclusions

1. As was found on the fast spreading EPR at 9–10°N, the most densely fissured regions within the Spike survey area (17°15′–40′S) lie within relatively older (age 2) terrains. In contrast, the least fissured areas coincide with where the freshest lavas are found. The positive correlation of fissure density with relative ages of axial lavas in the Spike survey area reveals the tendency of the crust in the axial zone to accumulate more cracks with time rather than to widen and deepen existing cracks [*Wright et al.*, 1995a]. This implies that the formation of wide, deep cracks is intimately related to episodes of dike intrusion, perhaps the lateral propagation of dikes, the eruption of fresh, uncracked flows, and hydrothermal venting. As intrusions and eruption wane, crustal cooling and extension produce additional smaller, shallower cracks in the frozen volcanic carapace overlying the sheeted dikes.

2. The majority of fissures along the Spike survey area may be generated by dike intrusions. At superfast spreading ridges our data appear to support dike intrusion and then lateral propagation rather than vertical injection from a greater abundance/frequency of eruptions in spatially distributed areas. Many fissures are estimated to penetrate the layer 2A/2B boundary and thus be deep enough to tap melt in places and to serve as loci for high-temperature hydrothermal discharge above the intrusions. There may be two major zones of lateral dike propagation from local sites of melt injection: one extending southward through the Aldo Lake and Tubeworm Segments, from 17°25′S down to 17°34′S, and a second zone that starts just to the south within the Stealth segment, between 17°37′S and 17°39′S. The focused hydrothermal flow is most abundant at the north ends of both of these zones.

3. The density of fissuring in the Spike area on the southern EPR is significantly higher than it is on the EPR at 9–10°N. Independent observations of lava flow morphology in these two areas by *Kurras et al.* [2000] and *White et al.* [2000, 2002] have demonstrated that there are comparatively more extensive lobate and sheet flows along the EPR crest at 9–10°N (i.e., lobate flows are the most abundant, but the relative percentage of area covered by sheet flows is higher along the EPR). These flows emanate from the axial summit collapse troughs found along most of the axial zone in this region. We suggest that these rather young, uncracked lobate and sheet flows are responsible for lower fissure density here in comparison to the Spike area on the southern EPR, where less effusive pillow flows of greater average lava age and higher fissure density are more common (in other words, the higher fissure density on the southern EPR fits well in explaining both the higher extensional rate and more frequent occurrence of pillow flows).

4. A distinct signature in crustal fissuring at a third- versus a fourth-order scale along superfast spreading ridges (as compared to fast spreading ridges) is not evident. Thinner crust at superfast spreading ridges may cause cracking events to propagate farther and affect multiple fine-scale segments at once, so that a second-order scale response is observed rather than a finer-scale third- or fourth-order signal. A greater frequency of diking and eruption (i.e., rapid, reconfiguration at shorter length and timescales) may create superpositions of distributions that are more difficult to deconvolve. Therefore it is may be more difficult to detect volcanic-hydrothermal-tectonic cycling (with fissure data at least) at superfast spreading rates, where volcanism is playing a much larger role in controlling seafloor morphology.

[29] **Acknowledgments.** The *Argo II* and DSL-120 technical groups of the Deep Submergence Laboratory, Woods Hole Oceanographic Institution, as well as Captain Eric Buck and crew of the R/V *Melville* and all the participants of the Sojourn 2 expedition are gratefully acknowledged for their enthusiastic help and cooperation. Dan Scheirer, Yves Lagabrielle, and Milene Cormier are thanked for helpful discussions. We thank Dan Scheirer for processing Imagenex data for us. The very careful and thoughtful reviews of Dan Fornari, an Associate Editor, and an anonymous reviewer significantly improved the manuscript. D.J.W. was supported by NSF grant OCE-9521039 and R.M.H., S.M.W., and K.C.M. by NSF/OCE-9416996 and NSF/OCE-9816021.

References

Auzende, J.-M., et al., Recent tectonic, magmatic, and hydrothermal activity on the East Pacific Rise between 17°S and 19°S: Submersible observations, *J. Geophys. Res.*, *101*, 17,995–18,010,1996.

Bäcker, H., J. Lange, and V. Marchig, Hydrothermal activity and sulfide formation in axial valleys of the East Pacific Rise crest between 18 and 22°S, *Earth Planet. Sci. Lett.*, *72*, 9–22, 1985.

Baker, E. T., and T. Urabe, The distribution of hydrothermal venting along the superfast-spreading East Pacific Rise, 13°30′–18°40′S, *J. Geophys. Res.*, *101*, 8685–8695, 1996.

Ballard, R. D., and J. Francheteau, The relationship between active sulfide deposition and the axial processes of the mid-ocean ridge, *Mar. Technol. Soc. J.*, *16*, 8–20, 1982.

Batiza, R., Magmatic segmentation of mid-ocean ridges: A review, in *Tectonic, Magmatic, Hydrothermal and Biological Segmentation of Mid-ocean Ridges*, edited by C. J. MacLeod, P. A. Tyler, and C. L. Walker, *Geol. Soc. Spec. Publ.*, *118*, 10–130, 1996.

Bohnenstiehl, D. R., and M. C. Kleinrock, Fissuring near the TAG active hydrothermal mound, 26°N on the Mid-Atlantic Ridge, *J. Volcanol. Geotherm. Res.*, *98*, 33–48, 2000.

Bowen, A., D. Fornari, J. Howland, and B. Walden, The Woods Hole Oceanographic Institution's remotely-operated and towed vehicle facilities for deep ocean research, Woods Hole Oceanogr. Inst., Woods Hole, Mass., 1993

Carbotte, S. M., J. C. Mutter, and L. Xu, Contribution of volcanism and tectonism to axial and flank morphology of the southern East Pacific Rise, 17°10′–17°40′S, from a study of layer 2A geometry, *J. Geophys. Res.*, *102*, 10,165–10,184, 1997.

Chadwick, W. W., Jr., and R. W. Embley, Graben formation associated with recent dike intrusions and volcanic eruptions on the mid-ocean ridge, *J. Geophys. Res.*, *103*, 9807–9826, 1998.

Christeson, G. L., G. M. Purdy, and G. J. Fryer, Seismic constraints on shallow crustal emplacement processes at the fast spreading East Pacific Rise, *J. Geophys. Res.*, *99*, 17,957–17,996, 1994.

Christeson, G. L., P. R. Shaw, and J. D. Garmany, Shear and compressional wave structure of the East Pacific Rise, 9°–10°N, *J. Geophys. Res.*, *102*, 7821–7836, 1997.

Collier, J. S., and S. C. Singh, Poisson's ratio structure of young oceanic crust, *J. Geophys. Res.*, *103*, 20,981–20,996, 1998.

Cormier, M.-H., and K. C. Macdonald, East Pacific Rise 18°–19°S: Asymmetric spreading and ridge reorientation by ultrafast migration of axial discontinuities, *J. Geophys. Res.*, *99*, 543–564, 1994.

Cormier, M.-H., D. S. Scheirer, and K. C. Macdonald, Evolution of the East Pacific Rise at 16°–19°S since 5 Ma: Bisection of overlapping spreading centers by new, rapidly propagating ridge segments, *Mar. Geophys. Res.*, *18*, 53–84, 1996.

Cormier, M.-H., W. B. F. Ryan, W. Jin, A. Shah, A. M. Bradley, D. R. Yoerger, H. Singh, J. Sinton, R. Batiza, and K. Rubin, Building of the extrusive crust of the EPR at 17 28′S through fissure-fed inflationary lava flows (abstract), *Eos Trans. AGU*, *80*(46), Fall Meet. Suppl. F1097, 1999.

Crane, K., Structural evolution of the East Pacific Rise axis from 13°10′N to 10°35′N: Interpretations from SeaMARC I data, *Tectonophysics*, *136*, 65–124, 1987.

Curewitz, D., and J. A. Karson, Geological consequences of dike intrusion at mid-ocean ridge spreading centers, in *Faulting and Magmatism at*

Mid-ocean Ridges, *Geophys. Monogr. Ser.,* vol 106, edited by W. R. Buck et al., pp. 11–136, AGU, Washington, D. C., 1998.
DeMets, C., R. G. Gordon, D. F. Argus, and S. Stein, Effect of recent revisions to the geomagnetic reversal time scale on estimates of current plate motions, *Geophys. Res. Lett.*, *21*, 2191–2194, 1994.
Detrick, R. S., A. J. Harding, G. M. Kent, J. A. Orcutt, and J. C. Mutter, Seismic structure of the southern East Pacific Rise, *Science*, *259*, 499–503, 1993.
Dziak, R. P., C. G. Fox, and A. E. Schreiner, The June-July 1993 seismoacoustic event at CoAxial segment, Juan de Fuca Ridge: Evidence for a lateral dike injection, *Geophys. Res. Lett.*, *22*, 135–138, 1995.
Embley, R. W., Geologic, chemical, and biological evidence for recent volcanism at 17.5°S: East Pacific Rise, *Earth Planet. Sci. Lett.*, *163*, 131–147, 1998.
Engels, J., Collapse of seafloor volcanic terrain: A key process in the formation of the upper oceanic crust, Master's thesis, Univ. of Hawai'i at Manoa, Honolulu, 2001.
Fialko, Y., On origin of near-axis volcanism and faulting at fast spreading mid-ocean ridges, *Earth Planet. Sci. Lett.*, *190*, 31–39, 2001.
Fornari, D. J., R. M. Haymon, M. R. Perfit, T. K. P. Gregg, and M. H. Edwards, Axial summit trough of the East Pacific Rise 9°–10°N: Geological characteristics and evolution of the axial zone of fast spreading mid-ocean ridges, *J. Geophys. Res.*, *103*, 9827–9856, 1998.
Forslund, T., and A. Gudmundsson, Crustal spreading due to dikes and faults in southwest Iceland, *J. Struct. Geol.*, *13*, 443–457, 1991.
Francheteau, J., R. Armijo, J.-L. Cheminée, R. Hékinian, P. Lonsdale, and N. Blum, Dyke complex of the East Pacific Rise exposed in the walls of Hess Deep and the structure of the upper oceanic crust, *Earth Planet. Sci. Lett.*, *111*, 109–121, 1992.
Fujioka, K., MODE '94: Active hydrothermal systems of a super-fast spreading ridge, southern East Pacific Rise (13°58′S to 18°26′S), *InterRidge News*, *4*, 7–10, 1995.
Garel, E., O. Dautiel, and Y. Lagabrielle, Deformation processes at fast to ultra-fast oceanic spreading axes: Mechanical approach, *Tectonophysics*, in press, 2002.
Gripp, A. E., and R. G. Gordon, Current plate velocities relative to the hot spots incorporating the NUVEL-1 plate motion model, *Geophys. Res. Lett.*, *17*, 1109–1112, 1990.
Gudmundsson, A., Tectonics of the Thingvellir fissure swarm, SW Iceland, *J. Struct. Geol.*, *9*, 61–69, 1987.
Gudmundsson, A., Emplacement of dikes, sills, and crustal magma chambers at divergent plate boundaries, *Tectonophysics*, *176*, 257–275, 1990.
Gudmundsson, A., Formation and growth of normal faults at the divergent plate boundary in Iceland, *Terra Nova*, *4*, 464–471, 1992.
Gudmundsson, A., and K. Bäckström, Structure and development of the Sveinagja Graben, northeast Iceland, *Tectonophysics*, *200*, 111–125, 1991.
Haimson, B. C., and F. Rummel, Hydrofracturing stress measurements in the Iceland research drilling project drill hole at Reydarfjördur, Iceland, *J. Geophys. Res.*, *87*, 6631–6649, 1982.
Haymon, R. M., The response of ridge-crest hydrothermal systems to segmented, episodic magma supply, in *Tectonic, Magmatic, Hydrothermal and Biological Segmentation of Mid-Ocean Ridges*, edited by C. J. MacLeod, P. A. Tyler, and C. L. Walker, *Geol. Soc. Spec. Publ.*, *118*, 157–168, 1996.
Haymon, R. M., D. J. Fornari, M. H. Edwards, S. Carbotte, D. Wright, and K. C. Macdonald, Hydrothermal vent distribution along the East Pacific Rise Crest (9°09′–54′N) and its relationship to magmatic and tectonic processes on fast-spreading mid-ocean ridges, *Earth Planet. Sci. Lett.*, *104*, 513–534, 1991.
Haymon, R. M., et al., Distribution of fine-scale hydrothermal, volcanic, and tectonic features along the EPR crest, 17°15′–18°30′S: Results of near-bottom acoustic and optical surveys (abstract), *Eos Trans. AGU*, *78*(46), Fall Meet. Suppl., F705, 1997.
Head, J. W., III, L. Wilson, and D. K. Smith, Mid-ocean ridge eruptive vent morphology and substructure: Evidence for dike widths, eruption rates, and evolution of eruptions and axial volcanic ridges, *J. Geophys. Res.*, *101*, 28,265–28,280, 1996.
Hey, R. N., P. D. Johnson, F. Martinez, J. Korenaga, M. L. Somers, Q. J. Huggett, T. P. LeBas, R. I. Rusby, and D. F. Naar, Plate boundary reorganization at a large-offset, rapidly propagating rift, *Nature*, *378*, 167–170, 1995.
Hooft, E. E. E., R. S. Detrick, and G. M. Kent, Seismic structure and indicators of magma budget along the southern East Pacific Rise, *J. Geophys. Res.*, *102*, 27,319–27,340, 1997.
Hussenoeder, S. A., J. A. Collins, G. M. Kent, R. S. Detrick, and T. Group, Seismic analysis of the axial magma chamber reflector along the southern East Pacific Rise from conventional reflection profiling, *J. Geophys. Res.*, *101*, 22,087–22,106, 1996.
Ito, H., Development of a borehole televiewer digital data acquisition system and fracture system observed in the Tanna Basin, *Rep.282*, pp. 29–316, Geol. Surv. of Jpn., Tsukuba, 1995.
Jaeger, J. C., and N. G. W. Cook, *Fundamentals of Rock Mechanics*, 3rd ed., Chapman and Hall, New York, 1979.
Johnson, H. P., and B. L. Salem, Magnetic properties of dikes from the oceanic upper crustal section, *J. Geophys. Res.*, *99*, 21,733–21,740, 1994.
Karson, J. A., S. D. Hurst, and P. Lonsdale, Tectonic rotations of dikes in fast-spread oceanic crust exposed near Hess Deep, *Geology*, *20*, 685–692, 1992.
Karson, J. A., E. M. Klein, and S. D. Hurst, Internal structure of uppermost fast-spread oceanic crust of the East Pacific Rise exposed at the Hess Deep rift: Results from Alvin, Argo II, and DSL 120 investigations (abstract), *Eos Trans. AGU*, *80*(46), Fall Meet. Suppl., F983–F984, 1999.
Krammer, A., P. Pezard, P. Harvey, K. H. Peter, and K. Fuchs, Borehole televiewer data analysis of Hole 504B from legs 137 and 140, *Proc. Ocean Drill. Program Sci. Results*, *137/140*, 29–304, 1995.
Kurras, G. J., D. J. Fornari, M. H. Edwards, M. R. Perfit, and M. C. Smith, Volcanic morphology of the East Pacific Rise crest 9°49′–52′: Implications for volcanic emplacement processes at fast-spreading mid-ocean ridges, *Mar. Geophys. Res.*, *21*(1/2), 23–41, 2000.
Lachenbruch, A. H., Depth and spacing of tension cracks, *J. Geophys. Res.*, *66*, 4273–4292, 1961.
Lachenbruch, A. H., A simple mechanical model for oceanic spreading centers, *J. Geophys. Res.*, *78*, 3395–3417, 1973.
Lagabrielle, Y., and M.-H. Cormier, Formation of large summit troughs along the East Pacific Rise as collapse calderas: An evolutionary model, *J. Geophys. Res.*, *104*, 12,971–12,988, 1999.
Lin, J., and E. M. Parmentier, Mechanisms of lithospheric extension at mid-ocean ridges, *Geophys. J.*, *96*, 1–22, 1989.
Lonsdale, P., Segmentation of the Pacific-Nazca spreading center, 1°N–20°S, *J. Geophys. Res.*, *94*, 12,197–12,225, 1989.
Lowell, R. P., and L. N. Germanovich, Dike injection and the formation of megaplumes at ocean ridges, *Science*, *267*, 1804–1807, 1995.
Macdonald, K. C., and P. J. Fox, The axial summit graben and cross-sectional shape of the East Pacific Rise as indicators of axial magma chambers and recent volcanic eruptions, *Earth Planet. Sci. Lett.*, *88*, 119–131, 1988.
Macdonald, K. C., P. J. Fox, L. J. Perram, M. F. Eisen, R. M. Haymon, S. P. Miller, S. M. Carbotte, M. -H. Cormier, and A. N. Shor, A new view of the mid-ocean ridge from the behaviour of ridge-axis discontinuities, *Nature*, *335*, 217–225, 1988.
Macdonald, K. C., D. S. Scheirer, and S.M. Carbotte, Mid-ocean ridges: Discontinuities, segments and giant cracks, *Science*, *253*, 986–994, 1991.
MacLeod, C. J., and D. A. Rothery, Ridge axial segmentation in the Oman ophiolite: Evidence from along-strike variations in the sheeted dike complex, in *Ophiolites and Their Modern Analogues*, edited by L. M. Parson, B. J. Murton, and P. Browning, *Geol. Soc. Spec. Publ.*, *60*, 3–63, 1992.
Magde, L. S., R. S. Detrick, and T. Group, Crustal and upper mantle contribution to the axial gravity anomaly at the southern East Pacific Rise, *J. Geophys. Res.*, *100*, 3747–3766, 1995.
Marchig, V., J. Erzinger, and P.-M. Heinze, Sediment in the black smoker area of the East Pacific Rise (18.5°S), *Earth Planet. Sci. Lett.*, *79*, 93–106, 1986.
Mastin, L. G., and D. D. Pollard, Surface deformation and shallow dike intrusion processes at Inyo Craters, Long Valley, California, *J. Geophys. Res.*, *93*, 13,221–13,235, 1988.
Mutter, J. C., S. M. Carbotte, W. Su, L. Xu, P. Buhl, R. S. Detrick, G. M. Kent, J. A. Orcutt, and A. J. Harding, Seismic images of active magma systems beneath the East Pacific Rise between 17°05′ and 17°35′S, *Science*, *268*, 391–395, 1995.
Naar, D. F., and R. N. Hey, Recent Pacific-Easter-Nazca plate motions, in *Evolution of Mid-ocean Ridges*, *Geophys. Monogr. Ser.*, vol. 57, edited by J. M. Sinton, pp. 9–30, AGU, Washington, D. C., 1989.
O'Neill, J. H., Geologic controls on distribution of hydrothermal vents on the superfast-spreading southern East Pacific Rise, Master's thesis, Univ. of Calif., Santa Barbara, 1998.
O'Neill, J. H., R. M. Haymon, K. C. Macdonald, and S. M. White, Hydrothermal vents at 17°25′S and 17°37′S on the superfast-spreading EPR (abstract), *Eos Trans. AGU*, *79*(45), Fall Meet. Suppl., F817, 1998.
Perram, L. J., M.-H. Cormier, and K. C. Macdonald, Magnetic and tectonic studies of the dueling propagating spreading centers at 20°40′S on the East Pacific Rise: Evidence for crustal rotations, *J. Geophys. Res.*, *98*, 13,835–13,850, 1993.
Pollard, D. D., P. T. Delaney, W. A. Duffield, E. T. Endo, and A. T. Okamura, Surface deformation in volcanic rift zones, *Tectonophysics*, *94*, 541–584, 1983.
Renard, V., R. Hekinian, J. Francheteau, R. D. Ballard, and H. Bäcker,

Submersible observations at the axis of the ultra-fast-spreading East Pacific Rise (17°30′ to 21°30′S), *Earth Planet. Sci. Lett.*, *75*, 339–353, 1985.

Rubin, A. M., Dike-induced faulting and graben subsidence in volcanic rift zones, *J. Geophys. Res.*, *97*, 1839–1858, 1992.

Rubin, A. M., and D. D. Pollard, Origins of blade-like dikes in volcanic rift zones, in *Volcanism in Hawaii*, edited by R. W. Decker, T. L. Wright, and P. H. Stauffer, *U.S. Geol. Surv. Prof. Pap.*, *1350*, 1449–1470, 1987.

Rubin, K. H., M. C. Smith, E. C. Bergmanis, M. R. Perfit, J. M . Sinton, and R. Batiza, Geochemical heterogeneity within mid-ocean ridge lava flows: Insights into eruption, emplacement and global variations in magma generation, *Earth Planet. Sci. Lett.*, *188*(3–4), 349–367, 2001.

Scheirer, D. S., and K. C. Macdonald, Variation in cross-sectional area of the axial ridge along the East Pacific Rise: Evidence for the magmatic budget of a fast spreading center, *J. Geophys. Res.*, *98*, 7871–7886, 1993.

Scheirer, D. S., K. C. Macdonald, D. W. Forsyth, S. P. Miller, D. J. Wright, M.-H. Cormier, and C. M. Weiland, A map series of the southern East Pacific Rise and its flanks, 15°S to 19°S, *Mar. Geophys. Res.*, *18*, 1–12, 1996a.

Scheirer, D. S., M. Cormier, K. C. Macdonald, R. M. Haymon, and S. White, Sojourn Leg 1: Completing the picture of the East Pacific Rise and its flanks in the MELT area (abstract), *Eos Trans. AGU*, *77*(46), Fall Meet. Suppl., F663, 1996b.

Scheirer, D. S., D. W. Forsyth, M.-H. Cormier, and K. C. Macdonald, Shipboard geophysical indications of asymmetry and melt production beneath the East Pacific Rise near the MELT experiment, *Science*, *280*, 1221–1224, 1998.

Scheirer, D. S., D. J. Fornari, S. E. Humphris, and S. Lerner, High-resolution seafloor mapping using the DSL-120 sonar system: Quantitative assessment of sidescan and phase-bathymetry data from the Lucky Strike segment of the Mid-Atlantic Ridge, *Mar. Geophys. Res.*, *21*(1/2), 121–142, 2000.

Shah, A., M.-H. Cormier, W. B. F. Ryan, W. Jin, A. M. Bradley, and D. R. Yoerger, High resolution 3-D map of the Earth's magnetic field at the EPR reveals dike outcrops and large-scale void space in extrusive layer (abstract), *Eos Trans. AGU*, *80*(46), Fall Meet. Suppl., F1074, 1999.

Shaw, P. R., Age variations of oceanic crust Poisson's ratio: Inversion and a porosity evolution model, *J. Geophys. Res.*, *99*, 3057–3066, 1994.

Sigurdsson, O., Surface deformation of the Krafla fissure swarm in two rifting events, *J. Geophys.*, *47*, 154–159, 1980.

Sinton, J. M., S. M. Smaglik, J. J. Mahoney, and K. C. Macdonald, Magmatic processes at superfast spreading oceanic ridges: Glass compositional variations along the East Pacific Rise, 13°–23°S, *J. Geophys. Res.*, *96*, 6133–6155, 1991.

Sinton, J., Volcanological investigations at superfast spreading: Results from R/V *Atlantis* cruise 3–31, *RIDGE Events*, *10*, 17–23, 1999.

Tada, H., P. C. Paris, and G. R. Irwin, *The Stress Analysis of Cracks Handbook*. Del Res. Corp., Hellertown, Pa., 1973.

Urabe, T., The effect of magmatic activity on hydrothermal venting along the superfast-spreading East Pacific Rise, *Science*, *269*, 1092–1095, 1995.

White, S. M., K. C. Macdonald, and R. M. Haymon, Basaltic lava domes, lava lakes, and volcanic segmentation on the southern East Pacific Rise, *J. Geophys. Res.*, *105*, 23,519–23,536, 2000.

White, S. M., R. Haymon, and K. Macdonald, Hydrothermal and volcanic response to fine-scale segmentation of the East Pacific Rise, *Eos Trans. AGU*, *82*(47), Fall Meet. Suppl., Abstract T12A–T9096, 2001.

White, S. M., R. M. Haymon, D. J. Fornari, M. R. Perfit, and K. C. Macdonald, Correlation between volcanic and tectonic segmentation at fast spreading ridges: Evidence from volcanic structures and lava flow morphology on the East Pacific Rise, 9°–10°N, *J. Geophys. Res.*, 10.1029/2001JB000571, in press, 2002.

Wright, D. J., Formation and development of fissures at the East Pacific Rise: Implications for faulting and magmatism at mid-ocean ridges, in *Faulting and Magmatism at Mid-ocean Ridges*, *Geophys. Monogr. Ser.*, vol. 106, edited by W. R. Buck et al., pp. 137–151, AGU, Washington, D. C., 1998.

Wright, D. J., R. M. Haymon, and D. J. Fornari, Crustal fissuring and its relationship to magmatic and hydrothermal processes on the East Pacific Rise crest (9°12′–54′N), *J. Geophys. Res.*, *100*, 6097–6120, 1995a.

Wright, D. J., R. M. Haymon, and K. C. Macdonald, Breaking new ground: Estimates of crack depth along the axial zone of the East Pacific Rise (9°12′–54′N), *Earth Planet. Sci. Lett.*, *134*, 441–457, 1995b.

R. M. Haymon and K. C. Macdonald, Department of Geological Sciences, University of California, Santa Barbara, CA 93106, USA. (haymon@magic.geol.ucsb.edu; macdonald@geol.ucsb.edu)

S. M. White, Department of Geological Sciences, University of South Carolina, 701 Sumter St., Columbia, SC 29208, USA.

D. J. Wright, Department of Geosciences, Oregon State University, 104 Wilkinson Hall, Corvallis, OR 97331-5506, USA. (dawn@dusk.geo.orst.edu)